

## Directional magnetization effects in magnetic circular dichroism spectra of Fe

Hartmut Höchst,<sup>1</sup> Dennis Rioux,<sup>2</sup> Dai Zhao,<sup>3</sup> and David L. Huber<sup>3</sup>

<sup>1</sup>*Synchrotron Radiation Center, University of Wisconsin–Madison, 3731 Schneider Drive, Stoughton, Wisconsin 53589*

<sup>2</sup>*Physics Department, University of Wisconsin–Oshkosh, Oshkosh, Wisconsin*

<sup>3</sup>*Physics Department, University of Wisconsin–Madison, Madison, Wisconsin*

(Received 21 August 2001; published 23 January 2002)

Magnetic circular dichroism (MCD) spectra exhibit distinctively different spectral and angular variations that depend strongly on the interacting geometry defined by the propagation vector of the radiation, the direction of magnetization  $\mathbf{M}$ , and the angle of incidence  $\theta_i$ . Two extreme cases for MCD measurements around the Fe  $M_{2,3}$  region, where the magnetization is either parallel (longitudinal geometry) or perpendicular (polar geometry) to the surface, are presented and compared with theoretical predictions based upon the classical Fresnel formalism for reflections. The magnetic properties of Fe were modeled by a frequency-dependent, complex dielectric tensor  $\epsilon(\omega)$ . Agreement between the model predictions and the reflection MCD measurements performed in both polar and longitudinal geometries demonstrates the validity of this approach.

DOI: 10.1103/PhysRevB.65.064439

PACS number(s): 75.90.+w, 78.20.Ls

### I. INTRODUCTION

The orientation of magnetization relative to the surface of a film or its crystalline lattice is an important material parameter which modern magnetism tries to tailor by means of artificially made thin-film structures. For example, in technologies such as magneto-optical drives, the magnetic moments are aligned perpendicular to the surface in order to take advantage of the polar magneto-optical Kerr effect. Other systems that rely on a specific magnetization geometry include spin valves, compound ferromagnetic and ferrimagnetic substances that are often composed of elemental sublattices with distinct magnetic orientations, and magnetic multilayer structures that depend on orientation-dependent ferromagnetic coupling.<sup>1</sup>

The magnetization orientation is determined by the magnetocrystalline anisotropy energy (MAE). In thin films and multilayers the MAE frequently changes direction from a preferential in-plane orientation to a perpendicular direction. The magnetic anisotropy is proportional to the expectation value of the orbital magnetic moment, which depends strongly on the character of states close to the Fermi level.<sup>2</sup> A variety of tools exist that enable materials scientists to determine the spatial magnetic texture in these types of materials, including spin-polarized secondary electron emission spectroscopy, neutron diffraction, and magnetic circular dichroism (MCD).<sup>3–7</sup> Among the various optical techniques the magneto-optical Kerr effect gained popularity after some pioneering experiments explained on the basis of first-principle band-structure calculations.<sup>8</sup>

While the MAE is a ground-state property of the crystal, the magneto-optical anisotropy is a result of electronic excitations, and is related to spin and orbital polarizations of the initial and final states. Magnetic dichroism is a consequence of the dependence of the optical conductivity tensor  $\sigma(\omega)$  on the magnetic states, and manifests itself in the x-ray regime in the corresponding scalar absorption coefficient  $\mu(\omega)$  which in effect is the absorption cross section from a specific core state. The absorption coefficient is a direct measure of

the integrated final-state partial-density of states (DOS) into which dipole-allowed transitions are selected from a specific core edge. Erskine and Stern were the first to predict MCD effects in the  $M_{2,3}$  edge of Ni.<sup>9</sup> Because of the  $p \rightarrow d$  dipole selection rule the near-edge excitation will yield information on the empty  $d$ -like DOS. However, since the MCD effect depends strongly on the spin-orbit coupling in the initial state and to a lesser degree on the exchange splitting of the final state, experimenters frequently chose  $L_{2,3}$  edges whose larger spin-orbit interaction significantly simplifies the general MCD spectra.

During the last few years, x-ray MCD experiments utilizing synchrotron radiation sources quickly evolved into a widely used, element-specific technique to investigate the formation of magnetic moments in ferromagnetic, ferrimagnetic, and antiferromagnetic systems. Indeed, with the growing interest in this technique, theoretical advances have led to sum-rule models that conveniently decompose the dichroism signal into orbit  $\langle L_z \rangle$  and spin  $\langle S_z \rangle$  contributions<sup>10–15</sup> in addition to advances in experimental techniques.<sup>16,17</sup> While these models appear to be fairly accurate in describing many body aspects of the MCD process in  $L_{2,3}$  transitions, there seems to be less understanding of how other factors, such as the choice of a particular interaction geometry, influence MCD spectra and alter the quantitative moment analysis.<sup>18–20</sup> In order for magnetic circular dichroism to be a unique tool for determining the orientation of  $\mathbf{M}$ , as well as the magnitude of magnetic moments in these materials, a connection between experimentally observed features of MCD spectra and magnetic geometry of the sample must be made.

The present paper discusses the differences between two basic MCD geometries defined by the relative orientation of the magnetization vector  $\mathbf{M}$  with respect to the plane of incidence and the plane of the sample surface. In the longitudinal geometry shown in Fig. 1(a),  $\mathbf{M}$  is parallel to the plane of incidence and parallel to the reflecting surface. For the polar geometry the magnetization vector is also parallel to the plane of incidence, but in this case the magnetic moments

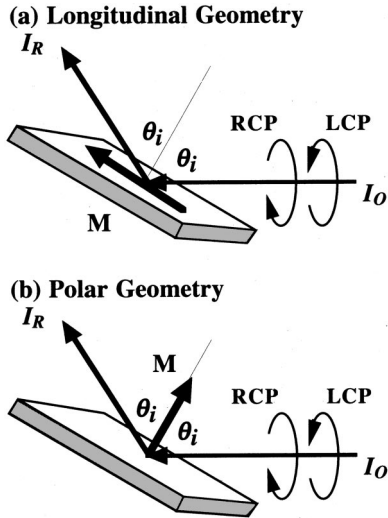


FIG. 1. Geometries for studying magneto-optical effects. Left (LCP) and right circularly polarized (RCP) light is incident at an angle  $\theta_i$  with respect to the surface normal, defining a plane of incidence. (a) In the longitudinal geometry the magnetization vector  $\mathbf{M}$  of the sample lies in the plane of incidence and parallel to the sample surface. (b) In the polar geometry the magnetization vector  $\mathbf{M}$  lies in the plane of incidence and perpendicular to the sample surface.

are perpendicular to the sample surface as indicated in Fig. 1(b). These geometries give rise to distinct energy- and angle-dependent dichroism signals, and might be useful for future studies investigating the element-specific orientations and magnetic moments in sublattices of compound ferrimagnets and antiferromagnets.

Due to the lack of suitable calculations modeling the frequency-dependent soft-x-ray-absorption coefficient relevant for the  $M_{2,3}$  MCD effect, we chose to analyze our results based on the classical Fresnel formalism for reflection. This approach allows one to use simple reflected-light intensity measurements to infer the frequency dependence of the off-diagonal elements  $\epsilon_{xy}(\omega)$  of the dielectric tensor that governs the response of the ferromagnetic medium to electromagnetic radiation. These results, which came from the longitudinal experimental geometry in this study, are then used to predict the magnitude of the MCD effect for the polar geometry. The predictions are verified by measurements, confirming the self-consistent nature of the formalism.

## II. EXPERIMENT

MCD spectra were collected at the University of Wisconsin Synchrotron Radiation Center using monochromatic, circularly polarized x rays supplied by a quadruple reflection polarizer (QRP) (Ref. 21) attached to the exit mirror box of the Amoco 6m toroidal grating monochromator.<sup>22</sup> The QRP supplies left (LCP) and right circularly polarized (RCP) light by inducing phase shifts between *s*- and *p*-polarized components of monochromatic, linearly polarized light reflected from four successive gold-coated mirrors. The optimum polarization performance is obtained in the energy range  $h\nu$

$=5\text{--}100$  eV. The QRP was operated in a mode that maximized the degree of circular polarization  $P_c$ . For these experiments  $P_c \approx 0.98$  over a range of photon energies about the Fe  $M_{2,3}$  absorption edge. Further details about the design and optical performance of the QRP are reported elsewhere.<sup>23,24</sup>

Thin Fe films were deposited in vacuum on a nonmagnetic substrate using a molecular-beam-epitaxy effusion cell. The films were magnetized in longitudinal or polar orientations by rare-earth permanent magnets mounted on the sample holder. The magnetic field at the film was  $\approx 3$  kG. MCD spectra at the  $M_{2,3}$  absorption edge were obtained by measuring the reflected light intensities for LCP and RCP light using a Si diode. The sample and detector assemblies could be rotated around a common axis with respect to the sample normal.

The lateral resolution of the QRP is directly related to the refocused spot size of the synchrotron light and the angle of incidence with respect to the sample surface. For the current study the light source had horizontal widths of  $\approx 0.5$  and  $0.1$  mm vertically. The illuminated vertical width at the sample varies with the angle of incidence by  $1/\cos(\theta_i)$ . The vertical beam size can be reduced to  $\approx 20$   $\mu\text{m}$  once the QRP is installed at its design location at the undulator beam line on port No. 071 at the Synchrotron Radiation Center.

## III. OUTLINE OF MAXWELL-FRESNEL THEORY

The intensities of LCP and RCP light reflected from ferromagnetic films differ near core absorption edges due to the polarization-dependent complex index of refraction, resulting in a dichroism. MCD spectra taken at an absorption edge will depend not only on the angular orientation of the magnetization vector  $\mathbf{M}$  with respect to the sample surface, but also on the reflected intensities  $I_R$  and  $I_L$  which vary as a function of the angle of incidence  $\theta_i$ . These contributions can be modeled within the established framework of the classical Fresnel-Maxwell equations.<sup>25</sup> Using this approach allows the development of a set of equations that directly relate the angular and helicity dependencies of the reflected light intensity to the dielectric properties of the reflecting film. The drawback of this approach is that the extraction of magnetic properties in terms of magnetic moments is not straightforward since the material properties are folded into the dielectric response function of the magnetized solid.

Assuming a semi-infinite solid with a complex refractive index given by

$$N = n - ik, \quad (1)$$

where  $n$  is the index of refraction and  $k$  the extinction coefficient, and defining the complex refraction angle  $\chi$  by

$$\sin(\chi) = \frac{\sin(\theta_i)}{N}, \quad (2)$$

allows one to solve equations for the reflection coefficients

which satisfy the boundary and phase conditions at the sample-vacuum interface. Incorporating circularly polarized light into the analysis is achieved by separating left and right circularly polarized radiation into  $s$ - and  $p$ -polarized components (based on the plane of incidence defined in Fig. 1) using a change in basis

$$\begin{bmatrix} A_s \\ A_p \end{bmatrix} = \begin{bmatrix} 1 \\ \pm i \end{bmatrix} A_o, \quad (3)$$

where  $\pm$  refers to RCP and LCP light of real amplitude  $A_o$ . For the longitudinal experimental geometry, the reflection coefficients can be shown to be given by the relations<sup>25</sup>

$$R_p = \frac{N \cos(\theta_i) - \cos(\chi)}{N \cos(\theta_i) + \cos(\chi)} A_p - \frac{\epsilon_{xy} \cos(90 - \alpha + \chi) \cos(\theta_i)}{N \cos(\chi) [N \cos(\theta_i) + \cos(\chi)] [N \cos(\chi) + \cos(\theta_i)]} A_s, \quad (4)$$

$$R_s = \frac{N \cos(\theta_i) - \cos(\chi)}{N \cos(\theta_i) + \cos(\chi)} A_s - \frac{\epsilon_{xy} \cos(90 - \alpha - \chi) \cos(\theta_i)}{N \cos(\chi) [N \cos(\theta_i) + \cos(\chi)] [N \cos(\chi) + \cos(\theta_i)]} A_p, \quad (5)$$

where  $\alpha$  is the angle between the magnetization vector and the sample surface. In Eqs. (4) and (5),  $\epsilon_{xy}$  are the frequency-dependent off-diagonal elements of the dielectric tensor, and account for the magnetic properties of the material. For a cubic ferromagnet magnetized in the  $z$  direction, the dielectric tensor can be written as

$$\epsilon = \begin{bmatrix} \epsilon_{xx} & \epsilon_{xy} & 0 \\ -\epsilon_{xy} & \epsilon_{yy} & 0 \\ 0 & 0 & \epsilon_{zz} \end{bmatrix}, \quad (6)$$

neglecting terms of order  $M^2$  and higher.<sup>9</sup> The diagonal elements account for the normal, isotropic response of the medium to electromagnetic radiation, and  $\epsilon_{xx}$  may be equivalent to  $\epsilon_{zz}$  if there are no magnetostrictive or other distortions of the lattice. In general,  $\epsilon_{xy}(\omega)$  is unknown. However, recording a MCD spectrum experimentally determines  $R_s$  and  $R_p$ , so that the frequency dependence of  $\epsilon_{xy}(\omega)$  can be obtained from a least squares fit of the experimental MCD data to the reflection equations [Eqs. (4) and (5)].

Since extension of the Fresnel-Maxwell model to other interaction geometries is trivial, reflection coefficient equations can be constructed and used in a predictive capacity. Once  $\epsilon_{xy}(\omega)$  has been determined, the reflected light intensities can be calculated from the complex reflection coefficients for different experimental geometries.<sup>25</sup>

#### IV. RESULTS AND DISCUSSION

The measured reflected-light intensities at each photon energy are converted here to an asymmetry ratio called the MCD effect, using the normalized value given by

$$\mathcal{M} = \frac{2(I_L - I_R)}{I_L + I_R} \quad (7)$$

where  $I_L$  and  $I_R$  are the reflected-light intensities for LCP and RCP light. When  $I_L$  and  $I_R$  are measured within seconds at each photon energy, as in our experiments, the MCD effect is independent of experimental conditions such as photon flux, that typically change from scan to scan.

Figure 2 presents plots of experimental MCD effect curves at the  $M_{2,3}$  absorption edge from Fe films magnetized in the longitudinal and polar geometries. Approximately 30 individual spectra each from the longitudinal and polar geometries are plotted together to demonstrate the dramatic variation in the MCD effect as a function of geometry, angle of incidence, and photon energy. Both interaction geometries exhibit regions of positive and negative MCD effect across different angle and energy ranges.

Figure 3 shows two representative MCD effect curves taken from the complete sets of data presented in Fig. 2. The top curve was taken in the longitudinal geometry using light from the monochromator-polarizer system to cover the full width of the absorption region around the  $M_{2,3}$  transition over an energy range of  $h\nu = 46\text{--}62$  eV. The angle of incidence was kept at  $\theta_i = 62.5^\circ$ . Approaching the edge from lower energies results in a negative MCD effect ( $I_L < I_R$ ) and above the edge the MCD effect is positive ( $I_L > I_R$ ). The bottom curve in Fig. 2 shows the MCD effect from a film magnetized along the sample normal in the polar geometry. In this case, the MCD effect is negative ( $I_L < I_R$ ) on both sides of the absorption edge.

Although the line shapes in Fig. 3 differ significantly from one another, there is nothing definitive in the shape of either curve that would allow us to conclude that the experimental geometry was polar or longitudinal or something in between. In other words, from a single MCD spectrum it is not possible to determine the orientation of the magnetic moments relative to the sample surface. However, the integrated area beneath these curves, in combination with the angle of incidence of the circularly polarized light, uniquely determines the orientation. The following discussion motivates this assertion.

A collection of MCD spectra like those in Fig. 2, encompassing the full parameter space defined by the angle of incidence and the photon energy in the longitudinal geometry, was analyzed using the macroscopic approach outlined above in order to determine  $\epsilon_{xy}(\omega)$ .<sup>24</sup> The diagonal elements  $\epsilon_{xx}(\omega) = \epsilon_{zz}(\omega)$  were taken from the literature.<sup>26</sup> This experimentally determined dielectric tensor was then used to predict the dependence of the polar MCD effect on the pho-

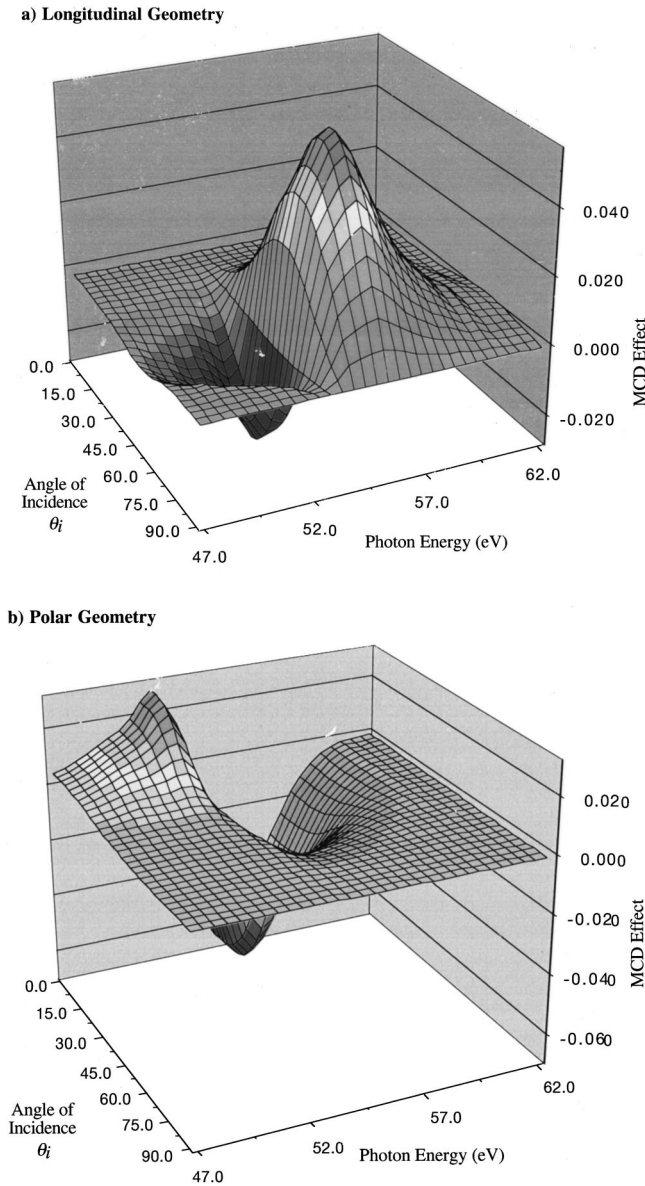


FIG. 2. MCD spectra taken from thick Fe films at the  $M_{2,3}$  absorption edge as a function of angle of incidence and photon energy for the (a) longitudinal and (b) polar geometries. The reported MCD signal is a normalized asymmetry ratio  $\mathcal{M} = 2 \times (I_L I_R) / (I_L + I_R)$  where  $I_L$  and  $I_R$  are reflected intensities for LCP and RCP light.

ton energy and angle of incidence. By inserting the experimentally determined dielectric tensor back into the reflection coefficient equations, theoretical MCD spectra for other geometries can be generated. Rather than concentrating on the detailed line shape, however, the MCD effect for the entire  $M_{2,3}$  absorption edge at a given angle of incidence can be collapsed into a single number by integrating the absolute area under the MCD spectrum, i.e., calculating the integral of  $|\mathcal{M}|$  over the absorption edge, where  $\mathcal{M}$  is defined in Eq. 7.

Figure 4 shows the predicted integrated area for Fe in both the polar and the longitudinal geometries, as calculated from the reflection coefficient equations using the dielectric model. Inspection of Fig. 4 reveals that for the two interac-

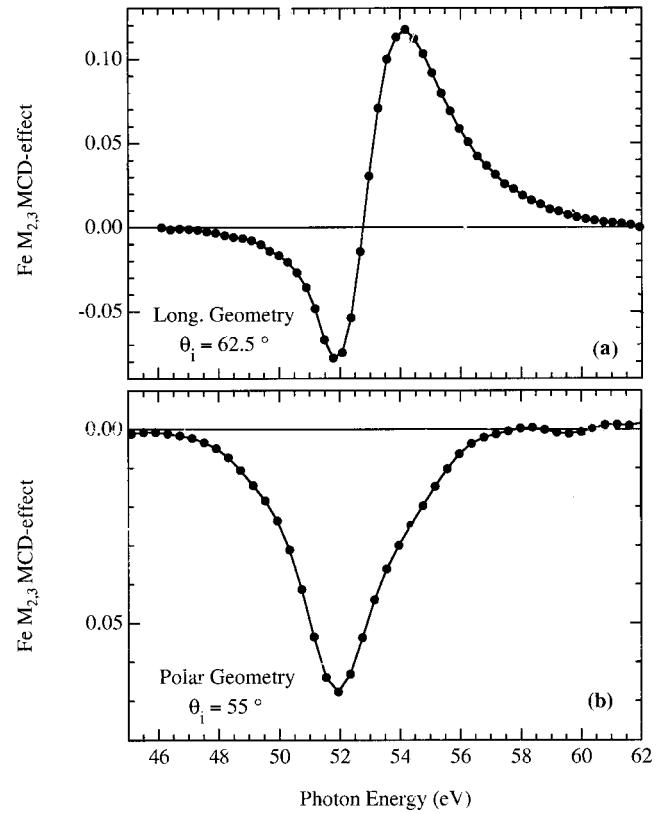


FIG. 3. Selected spectra from Fig. 2 showing details in variation of the MCD effect with photon energy and geometry. (a) MCD spectrum taken in the longitudinal geometry at  $\theta_i = 62.5^\circ$ . (b) MCD spectrum taken in the polar geometry at  $\theta_i = 55.0^\circ$ .

tion geometries the angular dependences of the integrated MCD effects are substantially different. While the polar MCD spectrum is close to its maximum value for  $\theta_i = 0^\circ$ , the longitudinal MCD spectrum maximizes around  $\theta_i = 58^\circ$ .

As a check on the self-consistency of our theoretical model, MCD experiments were performed in both polar and longitudinal geometries. Figure 5 shows a comparison of the measured and theoretically predicted integrated MCD values for both geometries (the theoretical and experimental values for the polar geometry have been scaled up by a factor of 2 for clarity). The angular range below  $\theta_i < 45^\circ$  was not utilized in the analysis for the polar geometry, because the absolute reflected intensities  $I_R$  and  $I_L$  drop off rapidly for those angles in the photon energy range of interest. Nevertheless, the observed agreement between the polar and longitudinal MCD experiments and their respective theoretical predictions establishes the validity of the classical dielectric model, and its utility in analyzing the angular dependence of reflection MCD spectra.

As noted earlier, the reflectivities in the longitudinal and polar geometries are direct functions of the diagonal and off-diagonal components of the frequency-dependent dielectric tensor. In recent years significant progress has been made in *ab initio* calculations to compute the frequency dependence of the optical conductivity tensor in layered crystalline ferromagnetic films as well as random alloy systems.<sup>27,28</sup> Using the same framework based on the Kubo-Greenwood linear-

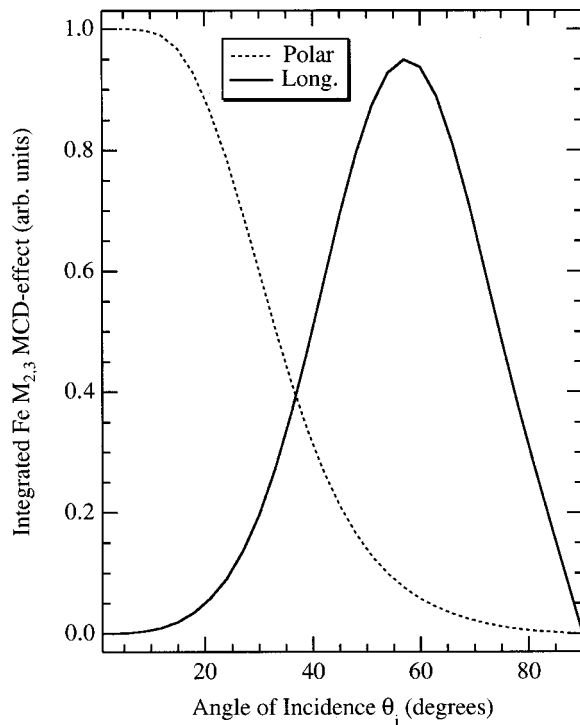


FIG. 4. Theoretical integrated MCD signals generated using the fitted dielectric constant based on a classical analysis of the longitudinal reflection MCD data. The absolute area beneath the MCD line shape at each angle of incidence is reported. Substantial differences between the polar and longitudinal geometries exist over much of the range of  $\theta_i$ .

response formalism, it should be possible to extend theory in order to calculate the frequency-dependent soft-x-ray conductivities or, equivalently, the complex dielectric tensor  $\epsilon(\omega)$ .

## V. CONCLUSIONS

MCD spectra of Fe films magnetized either in the film plane or perpendicular to the film surface exhibit characteristic differences with respect to the angle of incidence of the excitation radiation. The angular variations can be satisfactorily modeled within the Maxwell-Fresnel formalism. For magnetization directions that are between the longitudinal and polar cases, as in the sublattices of rare-earth intermetallic compounds<sup>29</sup> or for systems where the magnetization direction varies from in plane to perpendicular to the surface as function of superstructure film thickness,<sup>30</sup> the integrated MCD effect exhibits characteristic angular variations. These changes can be used to experimentally determine the angle of magnetization  $\alpha$  with respect to the sample surface. How-

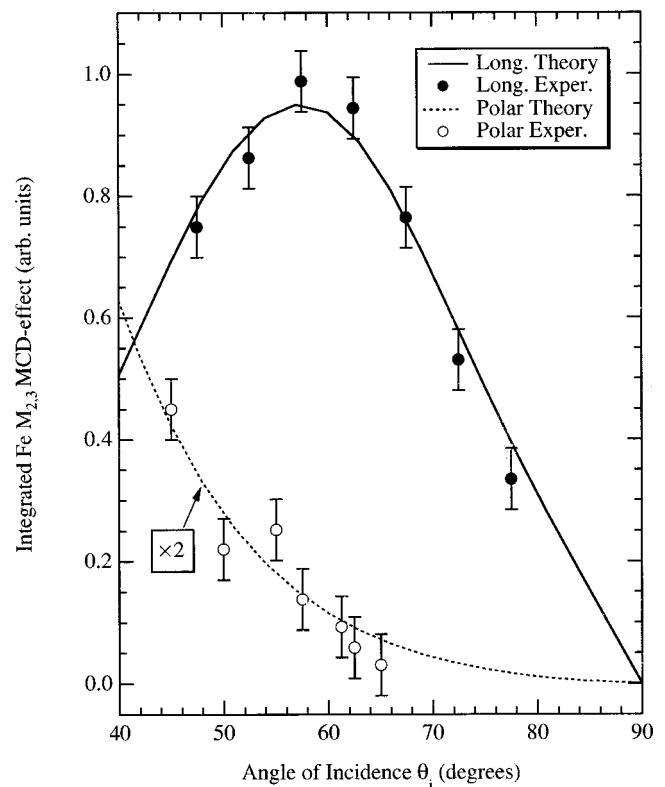


FIG. 5. Comparison between experimental and theoretical values for the energy integrated MCD effect from the polar and longitudinal geometries over the experimentally accessible angular range. The theoretical and experimental values for the polar geometry have been scaled up by a factor of 2 for clarity. The observed agreement establishes the validity of the classical Fresnel-Maxwell approach used here and demonstrates the utility of MCD in distinguishing magnetic moments aligned in the polar geometry from those in the longitudinal geometry.

ever, due to the lack of theoretical calculations of the dielectric tensor elements, a complete data set of MCD spectra must be measured at the absorption edge of each constituent element in order to determine the frequency dependence in the off-diagonal elements of the dielectric tensor otherwise needed in determining the magnetization angle  $\alpha$ .

## ACKNOWLEDGMENTS

This work was based upon research conducted at the Synchrotron Radiation Center, University of Wisconsin-Madison, which is supported by the NSF under Award No. DMR-0084402. This work was supported in part by a grant from Research Corporation under Award No. CC4139, and by the University of Wisconsin-Oshkosh Faculty Development Program.

<sup>1</sup>*Magnetic Anisotropy, Magnetization and Band Structure, Ultrathin Magnetic Structures*, edited by J.A.C. Bland and B. Heinrich (Springer, Berlin, 1994), Vol. 1, and references therein.

<sup>2</sup>P. Bruno, Phys. Rev. Lett. **39**, 865 (1989).

<sup>3</sup>D.P. Pappas, K.-P. Kämper, and H. Hopster, Phys. Rev. Lett. **64**, 3179 (1990).

<sup>4</sup>See, for example, B. D. Cullity, *Introduction to Magnetic Materials* (Addison-Wesley, Reading, MA, 1972).

- <sup>5</sup>J. Stöhr and Y. Wu, in *New Directions in Research with Third Generation Soft X-Ray Synchrotron Radiation Sources*, Vol. 254 of *NATO Advanced Study Institute, Series E: Applied Sciences*, edited by A.S. Schlachter and F.J. Wuilleumier (Kluwer Academic, Dordrecht, 1994), pp. 221-231.
- <sup>6</sup>Y.A. Uspenskii, E.T. Kulatov, and S.V. Halilov, *Phys. Rev. B* **54**, 474 (1996), and references therein.
- <sup>7</sup>L. Uba, S. Uba, V.N. Antonov, A.N. Yaresko, T. Slezak, and J. Korecki, *Phys. Rev. B* **62**, 13 731 (2000).
- <sup>8</sup>H. Ebert, *Rep. Prog. Phys.* **59**, 1665 (1996), and references therein.
- <sup>9</sup>J.L. Erskine and E.A. Stern, *Phys. Rev. B* **12**, 5016 (1975).
- <sup>10</sup>B.T. Thole, P. Carra, F. Sette, and G. van der Laan, *Phys. Rev. Lett.* **68**, 1943 (1992).
- <sup>11</sup>P. Carra, B.T. Thole, M. Altarelli, and X. Wang, *Phys. Rev. Lett.* **70**, 694 (1993).
- <sup>12</sup>R. Wu, D. Wang, and A.J. Freeman, *Phys. Rev. Lett.* **71**, 3581 (1993); R. Wu and A.J. Freeman, *ibid.* **73**, 1994 (1994).
- <sup>13</sup>G.Y. Guo, *Phys. Rev. B* **57**, 10 295 (1998).
- <sup>14</sup>D. Zhao, H. Höchst, and D.L. Huber, *J. Appl. Phys.* **84**, 2858 (1998).
- <sup>15</sup>A.I. Nesvizhskii, A.L. Ankudinov, and J.J. Rehr, *Phys. Rev. B* **63**, 094412 (2001).
- <sup>16</sup>R. Nakajima, J. Stöhr, and Y.U. Idzerda, *Phys. Rev. B* **59**, 6421 (1999).
- <sup>17</sup>E. Goering, A. Fuss, W. Weber, J. Will, and G. Schütz, *J. Appl. Phys.* **88**, 5920 (2000).
- <sup>18</sup>C.-C. Kao, C.T. Chen, E.D. Johnson, J.B. Hastings, H.J. Lin, G.H. Ho, G. Meigs, J.-M. Brot, S.L. Hulbert, Y.U. Idzerda, and C. Vettier, *Phys. Rev. B* **50**, 9599 (1994).
- <sup>19</sup>D. Rioux, B. Allen, H. Höchst, D. Zhao, and D.L. Huber, *Phys. Rev. B* **56**, 753 (1997).
- <sup>20</sup>G. van der Laan, *Phys. Rev. B* **57**, 5250 (1998).
- <sup>21</sup>H. Höchst, R. Patel and F. Middleton, *Nucl. Instrum. Methods Phys. Res. A* **347**, 107 (1994).
- <sup>22</sup>D.C. Mancini, M. Bissen, D. Rioux, R. Patel, G. Rogers, E. Brodsky, and H. Höchst, *Rev. Sci. Instrum.* **63**, 1269 (1992).
- <sup>23</sup>H. Höchst, P. Bulicke, T. Nelson, and F. Middleton, *Rev. Sci. Instrum.* **66**, 1598 (1995).
- <sup>24</sup>H. Höchst, D. Zhao, and D.L. Huber, *Surf. Sci.* **252-254**, 998 (1996).
- <sup>25</sup>D. Zhao, Ph.D. thesis, Department of Physics, University of Wisconsin–Madison, 1996.
- <sup>26</sup>J.J. Carroll, C.T. Ceyer, and A.J. Melmed, *J. Opt. Soc. Am.* **72**, 668 (1978).
- <sup>27</sup>T. Huhne, and H. Ebert, *Phys. Rev. B* **60**, 12 982 (1999).
- <sup>28</sup>J. Banhart, *Phys. Rev. Lett.* **82**, 2139 (1999).
- <sup>29</sup>F. Bourdarot, W. Hynn, E. Baggio-Saitovitch, Q. Huang, and S. Skanthakumar, *Phys. Rev. B* **64**, 104410 (2001).
- <sup>30</sup>R. Sellmann, H. Fritzsche, M. Maletta, V. Leiner, and R. Siebrecht, *Phys. Rev. B* **63**, 224415 (2001).